Supplementary Material

Materials and Methods. All chemicals were reagent grade, and used without further purification. All reactions were carried out under nitrogen atmosphere. Column chromatography was performed with Kanto Chemical silica gel 60 N (spherical, neutral) or Wako Chemical alumina (activated, about 200 mesh). Gel-permeation chromatography (GPC) was performed at room temperature using columns JAIGEL 2H-1H on a Japan Analytical Industry LC-908 recycling preparative HPLC system equipped with a variable-wavelength UV-vis detector. ^{1}H NMR spectra were recorded on a Bruker ARX400 spectrometer at 400 MHz, or a Bruker AC300 spectrometer at 300 MHz. ^{13}C NMR spectra were recorded on a Bruker ARX400 spectrometer at 100 MHz. In both NMR measurements, tetramethylsilane was used as an internal standard. Elemental analyses were carried out at the Chemical Analysis Center, University of Tsukuba, Japan. ESI-TOF (positive mode) mass spectra were recorded on an Applied Biosystems QStar Pulsar *i* spectrometer.

Synthesis. Aza-15-crown-ether was synthesized according to literature methods.[i] 2-(3'-bromophenyl)pyridine (85% yield) and 2-(4'-bromophenyl)pyridine (56% yield) were synthesized by classic Suzuki coupling of 2-bromo-pyridine with 3-bromophenyl- and 4-bromophenyl-boronic acid, respectively. The aza-15-crown-5 ether functionalized phenylpyridines **4** (64%) and **6** (42%) were obtained by Pd-catalyzed cross-coupling reactions of the corresponding bromophenylpyridine with aza-15-crown-5 ether.[ii]

Scheme S1: Synthesis of complex **1**

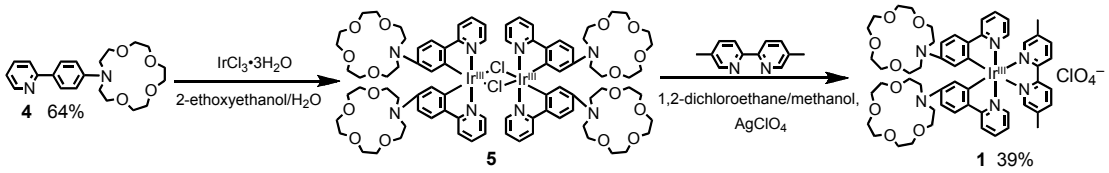

Synthesis of 13-(4-(pyridin-2-yl)phenyl)-1,4,7,10-tetraoxa-13-azacyclopentadecane (4). 2-(4-bromophenyl)pyridine (121 mg, 0.517 mmol), 1,4,7,10-tetraoxa-13-azacyclopentadecane (147 mg, 0.671 mmol) and sodium-*tert*-butoxide (61.7 mg, 0.642 mmol) were dissolved in 1.5 mL of toluene under nitrogen. $Pd(OAc)_2$ (3.90 mg, 0.0174 mmol), tri-*tert*-butyl phosphine (4 μL, 0.0165 mmol)

were dissolved in another flask with 1.5 mL of toluene under nitrogen and slowly added to the first solution. The combined solutions were refluxed for 12 hours. The mixture was poured onto water (15 mL), the phases were separated and the water phase extracted with ethyl acetate (15 mL × 3). The combined organic phases were washed with water, dried over Na_2SO_3, filtered and dried under vacuum. The crude material was purified by column chromatography (Al_2O_3, CH_2Cl_2/hexane (1:1, v/v) → CH_2Cl_2/MeOH (100:1, v/v)) followed by GPC to afford compound **4** (123 mg, 0.33 mmol) in 64% yield.

4 : deep yellow oil, ^{1}H NMR (400 MHz, $CDCl_3$) δ 3.64-3.69 (m, 16H), 3.79 (t, J = 6.2 Hz, 4H), 6.74 (d, J = 9.0 Hz, 2H), 7.10 (m, 1H), 7.62-7.67 (m, 2H), 7.89 (d, J = 9.0 Hz, 2H), 8.6 (d, J = 4.2 Hz,1H).

Synthesis of [Ir(4)$_2$(dmbpy)]ClO$_4$ (1). 4 (345 mg, 0.926 mmol) and $IrCl_3.3H_2O$ (112 mg, 0.319 mmol) in 2-ethoxyethanol/water (3:1) were degassed by 3 freeze dry cycles and refluxed at 110°C under nitrogen for 24h. After cooling to room temperature the solvent was evaporated, $CHCl_3$ was added and the mixture was filtered through celite. The solvent was evaporated and the [Ir(**4**)$_2$Cl]$_2$ dimer obtained was used without further purification.

[Ir(**4**)$_2$Cl]$_2$ (62.7 mg, 0.049 mmol), 5,5'-dimethyl-2,2'-bipyridine (13.2 mg, 0.0716 mmol) and silver perchlorate (13.2 mg, 0.0716 mmol) were dissolved in 1,2-dichloroethane/chloroform (2:1) and the mixture was degassed by 3 freeze dry cycle. The mixture was refluxed 3.5 hours under nitrogen and the crude product was purified by column chromatography (Al_2O_3, $CHCl_3$ → $CHCl_3$/MeOH (1:0 → 100:5, v/v)) to afford the desired complex **1** (38.3 mg, 0.0314 mmol) in 39% yield over two steps.

1: orange solid, ^{1}H NMR (400 MHz, $CDCl_3$) δ 2.30 (s, 6H), 3.37 (t, J = 5.8 Hz, 8H), 3.49-3.70 (m, 40H), 5.46 (d, J = 2.3 Hz, 2H), 6.34 (dd, J = 2.3, 8.7 Hz, 2H), 6.73 (t, J = 6.1 Hz, 2H), 7.34 (d, J = 6.1 Hz, 2H), 7.45 (d, J = 8.7 Hz, 2H), 7.52-7.62 (m, 4H), 7.78 (s, 2H), 7.93 (d, J = 8.3 Hz, 2H), 8.62 (d, J = 8.3 Hz, 2H). ^{13}C NMR (100 MHz, $CDCl_3$) δ 168.3, 153.6, 153.0, 150.1, 149.2, 148.0, 140.0, 138.2, 136.7, 131.2, 126.1, 124.4, 119.8, 117.4, 113.2, 106.1, 71.2, 70.2, 69.9, 68.4. ESI-MS *m/z* 1119.43 $[M]^+$. Anal. Calcd for $C_{54}H_{66}ClIrN_6O_{12}$ + 0.7 $CHCl_3$: C, 50.45; H, 5.16; N, 6.45. Found: C, 50.49; H, 5.26; N, 6.38.

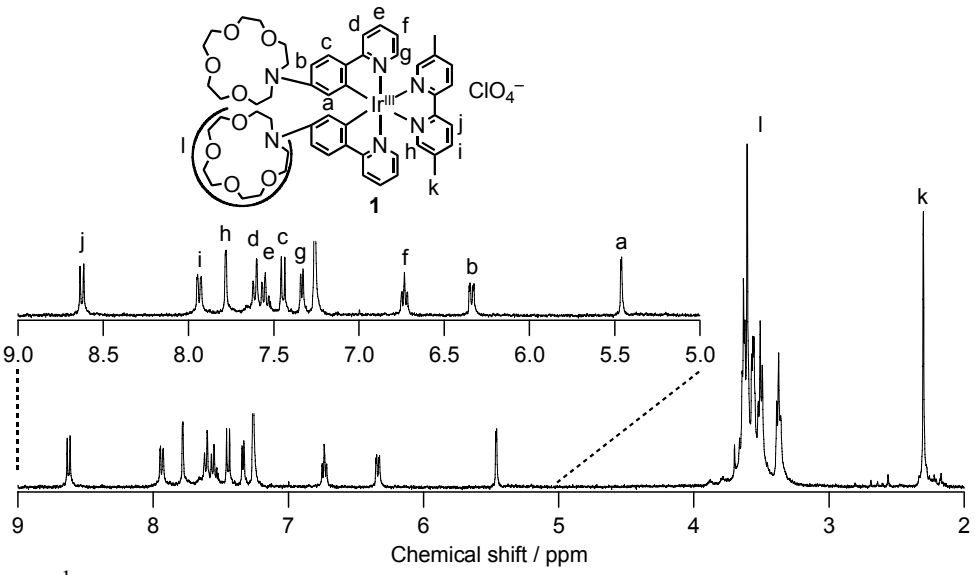

Figure S1: ^{1}H NMR spectrum of **1**, 400 MHz, $CDCl_3$

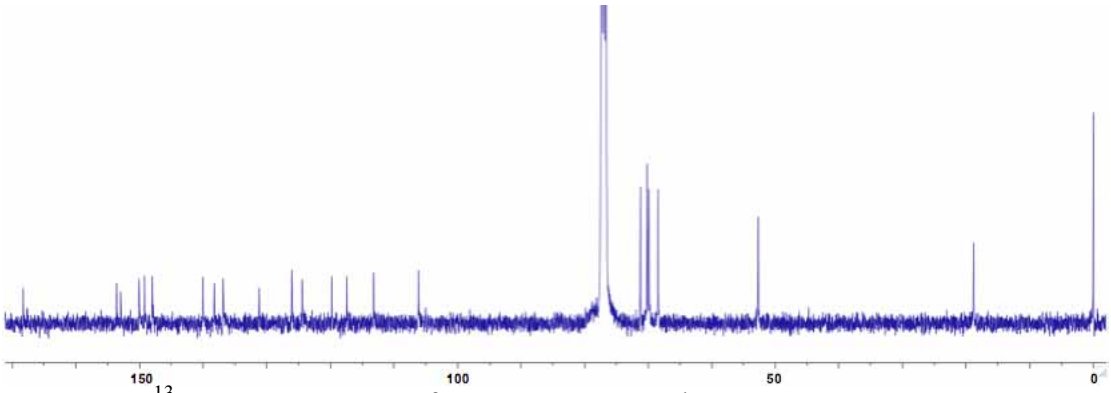

Figure S2: ^{13}C NMR spectrum of **1**, 100 MHz, $CDCl_3$

Scheme S2: Synthesis of complex 2.

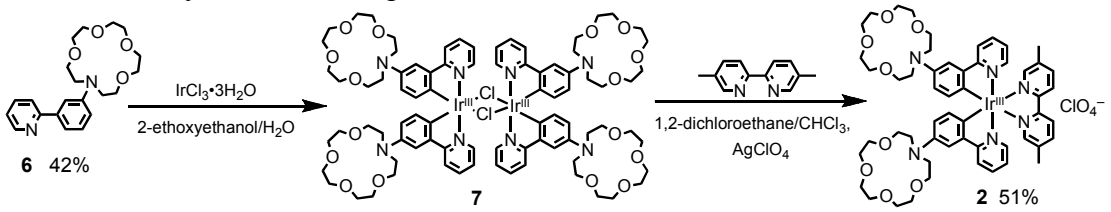

Synthesis of 13-(3-(pyridin-2-yl)phenyl)-1,4,7,10-tetraoxa-13-azacyclopentadecane (6). 2-(3-bromophenyl)pyridine (545 mg, 2.33 mmol), 1,4,7,10-tetraoxa-13-azacyclopentadecane (523 mg, 2.39 mmol) and sodium-*tert*-butoxide (286 mg, 2.97 mmol) were dissolved in 7 mL of toluene under nitrogen. $Pd(OAc)_2$ (15.7 mg, 70.1 μmol) and tri-*tert*-butyl palladium (63 μL, 0.26 mmol) were dissolved in another flask with 6.5 mL of toluene under nitrogen and slowly added to the first solution. The combined solutions were refluxed for 12 hours. The mixture

was poured onto water (40 mL), the phases were separated and the water phase extracted with ethyl acetate (40 mL × 3). The combined organic phases were washed with water (50 mL × 3), dried over Na_2SO_3 and dried under vacuum. The crude material was purified by column chromatography (Al_2O_3, CH_2Cl_2/hexane 1:1 → CH_2Cl_2/MeOH 100:1, v/v)) followed by GPC to afford compound **6** (364 mg, 0.98 mmol) in 42% yield.

6 : brown oil, ^{1}H NMR (400 MHz, $CDCl_3$) δ 3.64-3.70 (m, 16H), 3.81 (t, J = 6.1 Hz, 4H), 6.75 (dd, J = 8.1, 2.4 Hz, 2H), 7.19-7.32 (m, 3H), 7.68-7.75 (m, 2H), 8.67 (d, J = 4.6 Hz, 1H).

Synthesis of [Ir(6)$_2$(dmbpy)]ClO$_4$ (2). 6 (998.2 mg, 0.264 mmol), $IrCl_3.3H_2O$ (38.0 mg, 0.108 mmol) in 2-ethoxyethanol/water 3:1 were degassed by 3 freeze dry cycles and refluxed at 110 C under nitrogen for 24h. After cooling to room temperature, solvent was evaporated, $CHCl_3$ was added and the mixture was filtered through celite. The solvent was evaporated and the [Ir(**6**)$_2$Cl]$_2$ dimer obtained was used without further purification.

[Ir(**6**)$_2$Cl]$_2$ (54.6 mg), dmbpy (15.7 mg, 0.0852 mmol) and silver perchlorate (17.6 mg, 0.0852 mmol) were dissolved in 1,2-dichloromethane/$CHCl_3$ (2:1) and the mixture was degassed by 3 freeze dry cycles. The mixture was refluxed 3 hours under nitrogen and the crude product was purified by column chromatography (Al_2O_3, $CHCl_3$ → $CHCl_3$/MeOH 100:5, v/v) to afford the desired complex **2** (43.7 mg, 0.0359 mmol) in 51% yield over two steps.

2 : red orange solid, ^{1}H NMR (400 MHz, $CDCl_3$) δ 2.29 (s, 6H), 3.56 (t, J = 6.0 Hz, 8H), 3.63-3.68 (m, 24H), 3.75 (t, J = 6.0 Hz, 8H), 6.08 (d, J = 8.4 Hz, 2H), 6.46 (dd, J = 2.5, 8.4 Hz, 2H), 6.95 (t, J = 5.7 Hz, 2H), 7.03 (d, J = 2.5 Hz, 2H), 7.47 (d, J = 5.7 Hz, 2H), 7.69 (t, J = 7. 9 Hz, 2H), 7.74 (d, J = 1.8 Hz, 2H), 7.82 (d, J = 7.9 Hz, 2H), 7.93 (dd, J = 1.8, 8.4 Hz, 2H), 8.64 (d, J = 8.4 Hz, 2H). ^{13}C NMR (100 MHz, $CDCl_3$) δ 168.5, 150.1, 148.7, 144.4, 143.4, 140.1, 138.2, 137.3, 135.2, 131.8, 124.6, 122.8, 119.3, 116.3, 108.7, 71.3, 70.3, 70.1, 69.1. Anal. Calcd for $C_{54}H_{66}ClIrN_6O_{12}$ + 2 H_2O: C, 51.69; H, 5.62; N, 6.70. Found: C, 51.49; H, 5.44; N, 6.64.

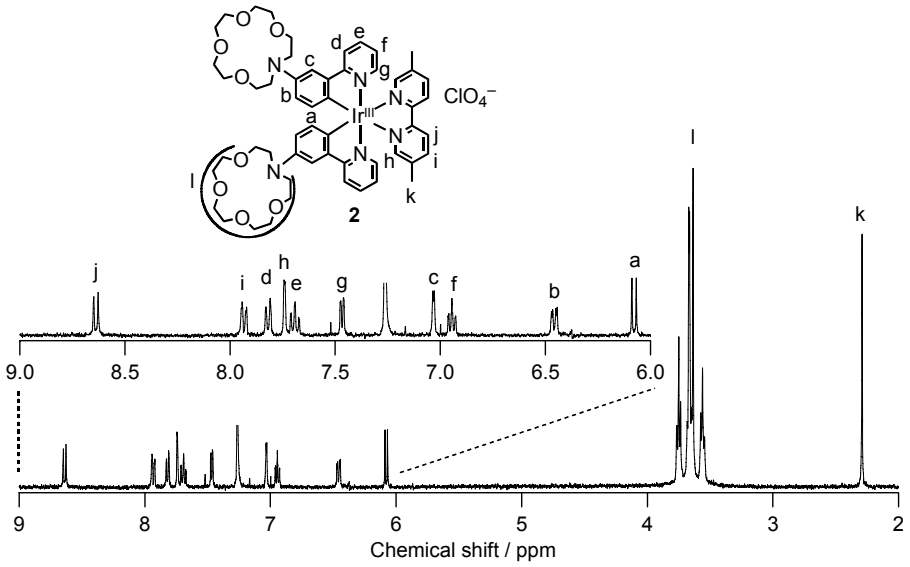

Figure S3: ^{1}H NMR spectrum of **2**, 400 MHz, $CDCl_3$

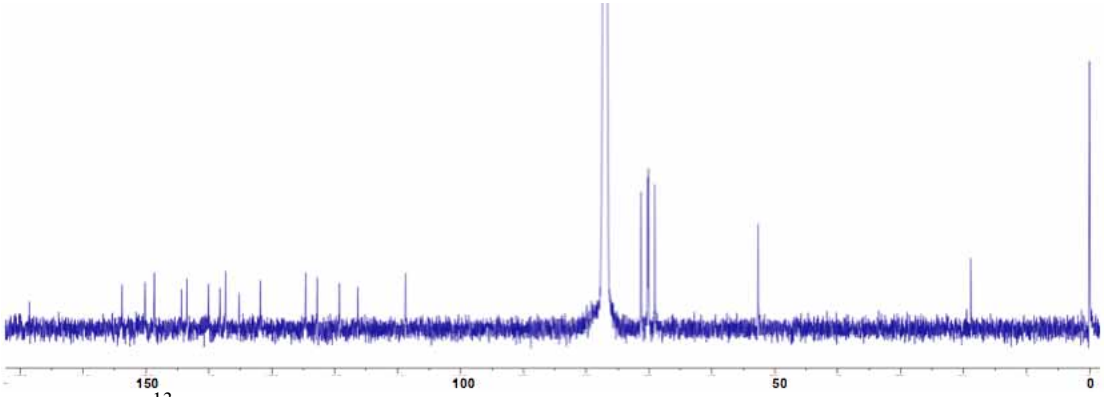

Figure S4: ^{13}C NMR spectrum of **2**, 100 MHz, $CDCl_3$

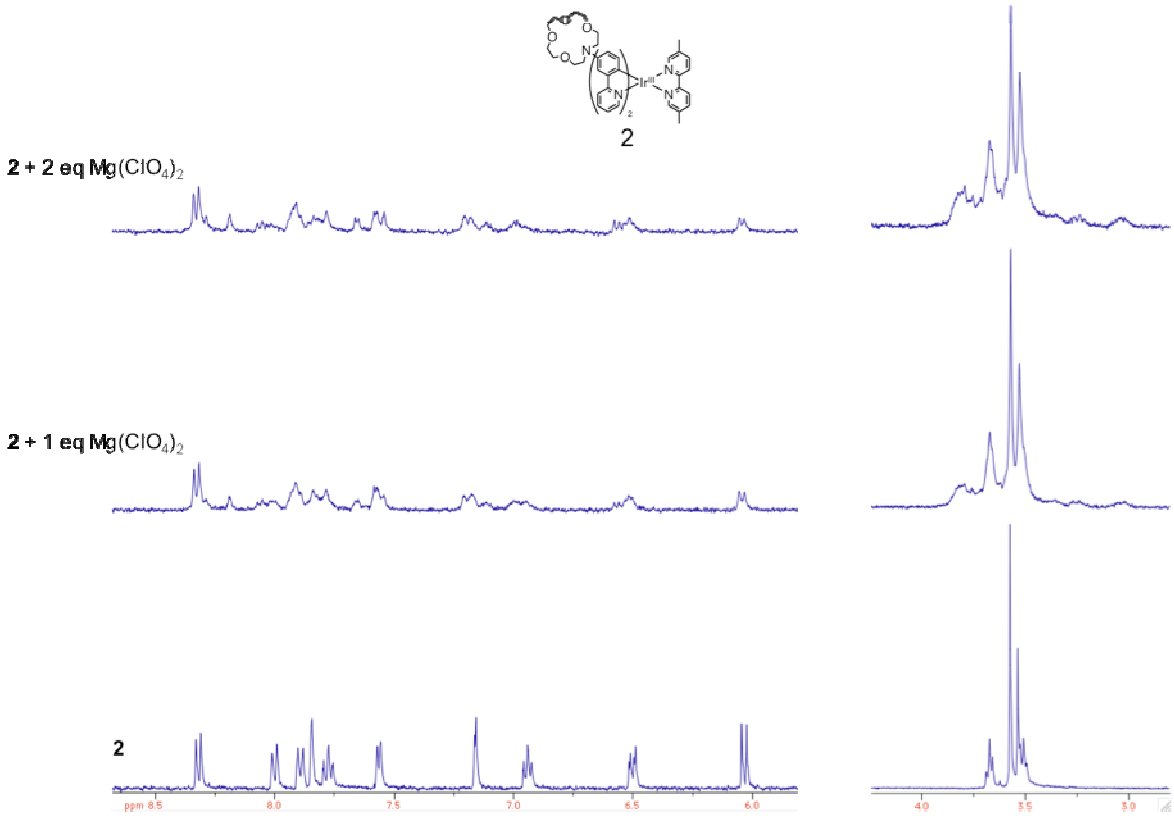

Figure S5: ^{1}H NMR spectral change of **2** in the presence of Mg^{2+}, 400 MHz, CD_3CN, 0.25 mM

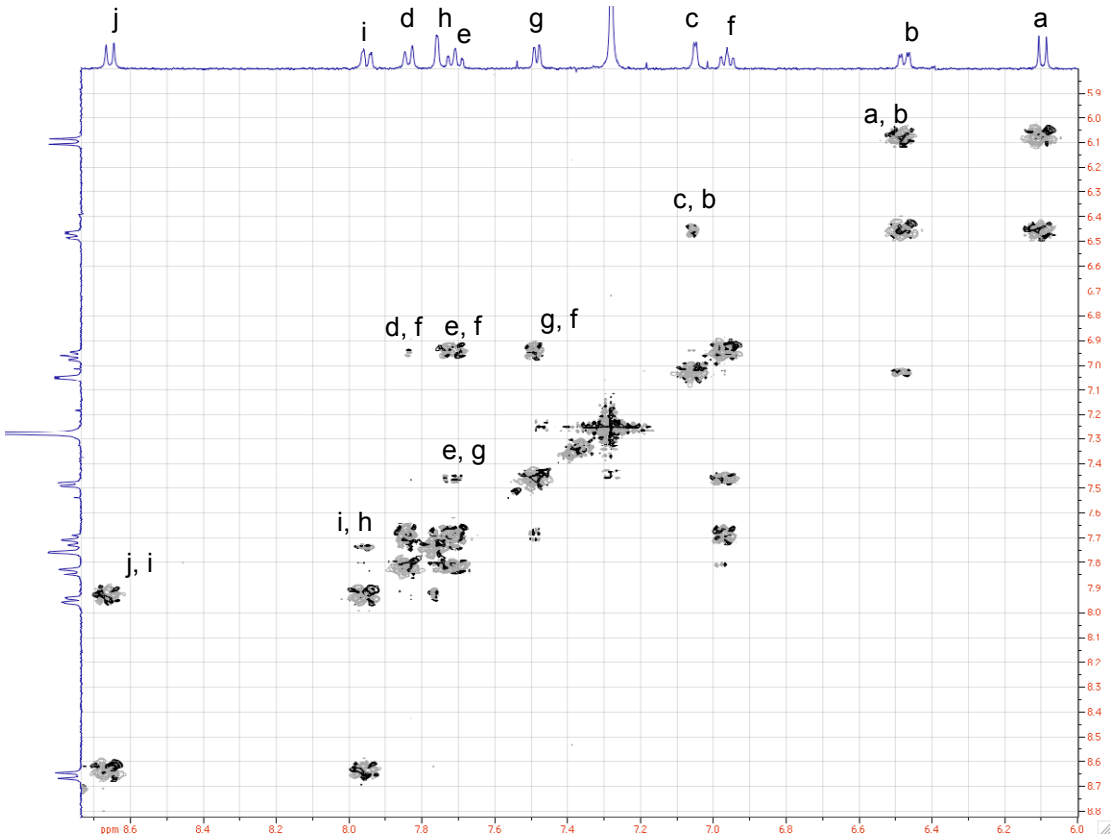

Figure S6: ^{1}H COSY NMR spectrum of **2**, 400 MHz, $CDCl_3$

Spectrophotometry. Absorption spectra were recorded on a JASCO V-660 spectrophotometer. Solutions (10^{-5} M) of the complexes in acetonitrile were placed in 1 cm quartz cuvettes and the titrations were performed by adding aliquots of metal perchlorate solutions. Emission spectra of ligands and their metallated complexes (A < 0.1 at the excitation wavelength) were recorded on a HITACHI F-4500 spectrofluorimeter and all samples were carefully degassed with argon prior to measurement. Emission titrations were performed similarly to the absorption titrations.

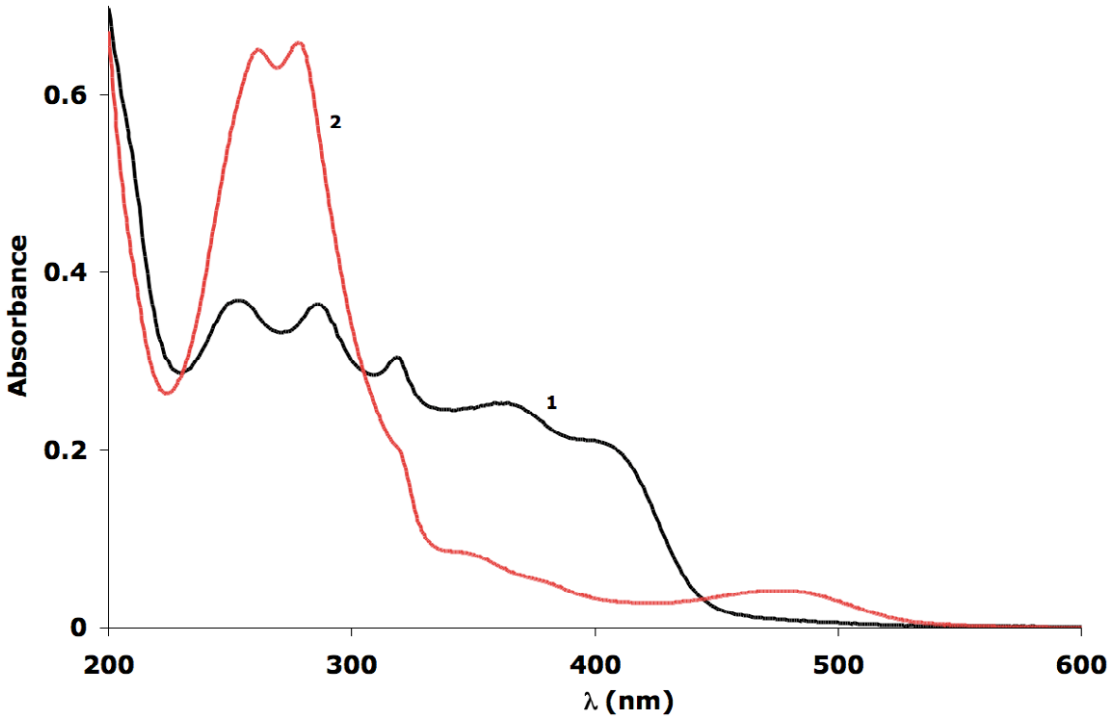

Figure S7. UV-Vis electronic spectra of free complexes **1** (black) and **2** (red) ([**1**] = [**2**] = 1.0×10^{-5} M) in degassed CH_3CN.

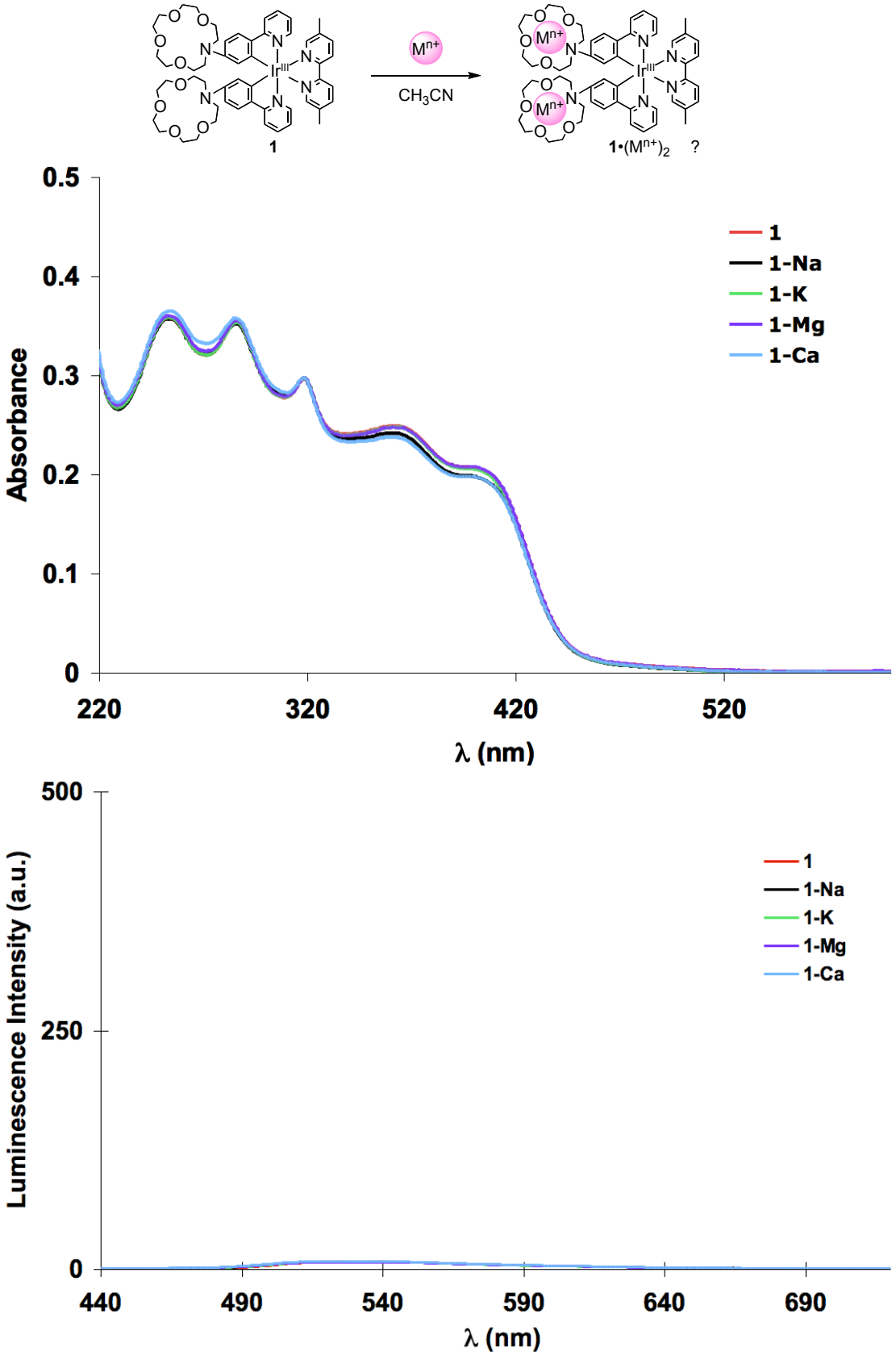

Figure S8. Absorption (top) and emission (bottom) spectra of **1** in the presence of excess of metal ions (Na^+, K^+, Mg^{2+}, Ca^{2+}). [**1**] = 1.0×10^{-5} M. λ_{ex} = 380 nm. CH_3CN.

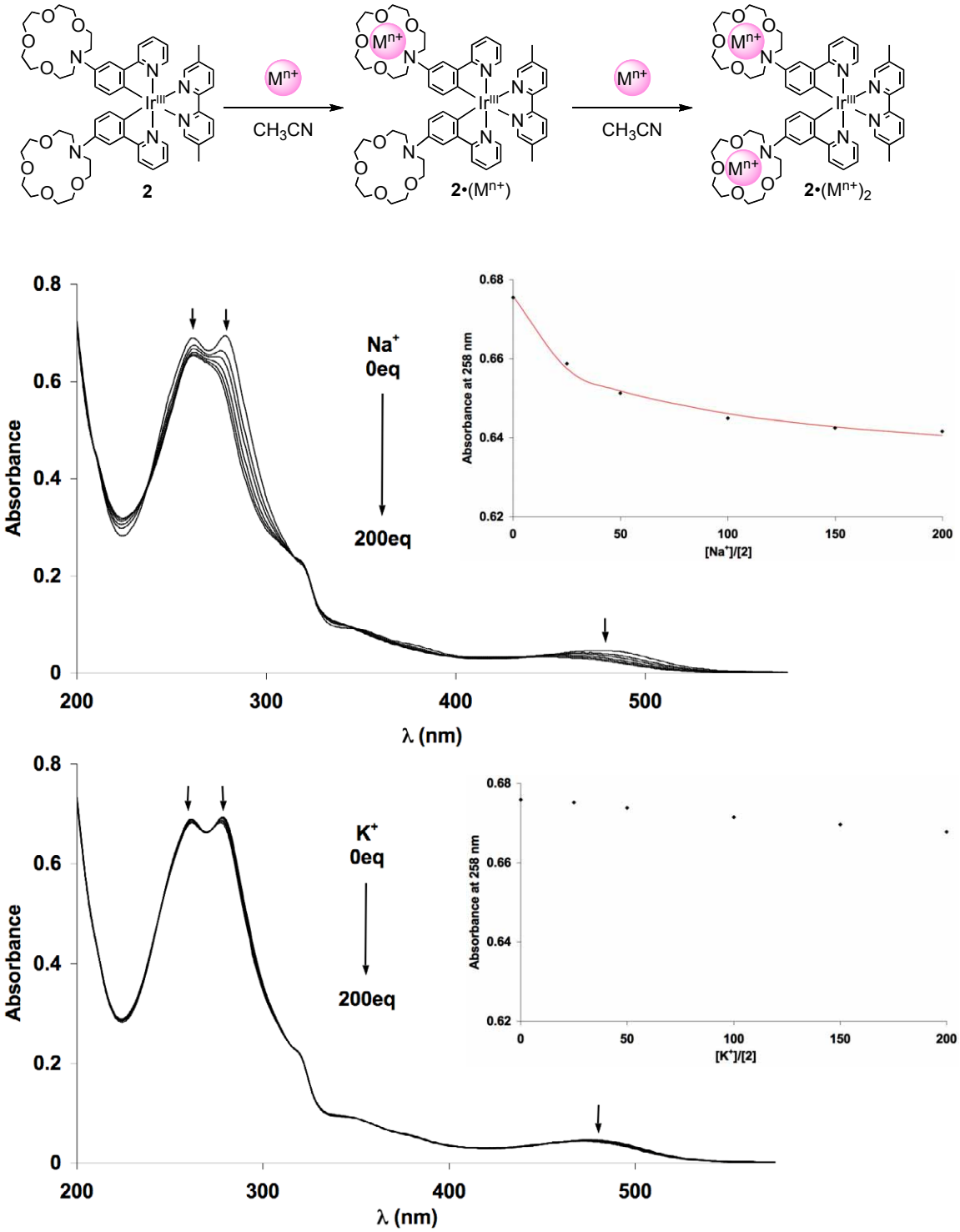

Figure S9. UV-visible titration of ligand **2** with sodium perchlorate (top) and potassium perchlorate (bottom). [**2**] = 1.0×10^{-5} M, CH_3CN. Inset shows the fit (red line) of the experimental data (black dots) at 258 nm.

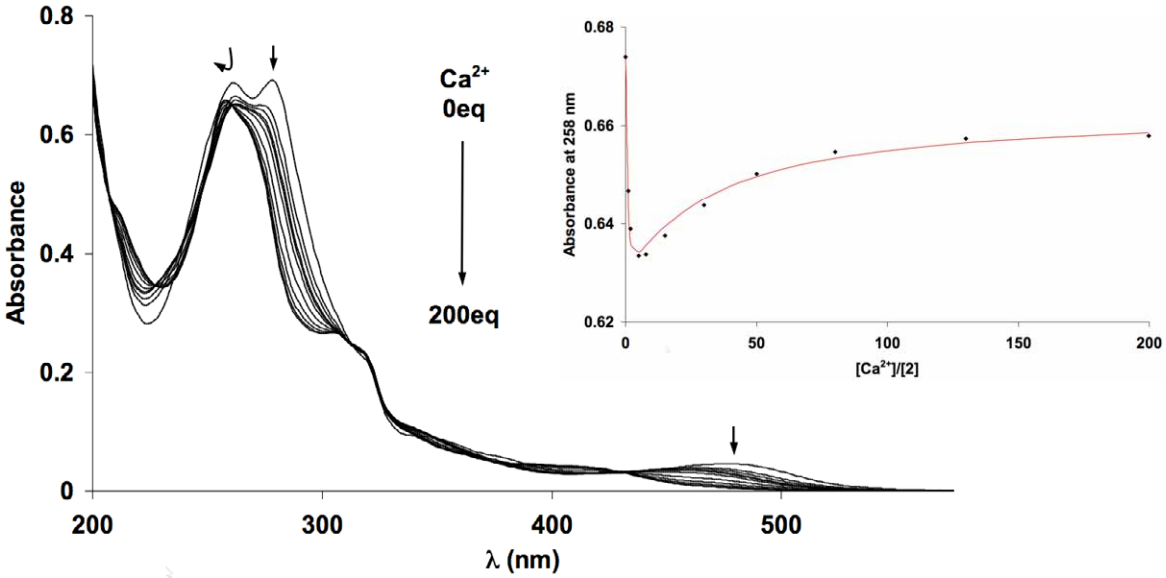

Figure S10. UV-visible titration of ligand **2** with calcium perchlorate. [**2**] = 1.0×10^{-5} M, CH_3CN. Inset shows the fit (red line) of the experimental data (black dots) at 258 nm.

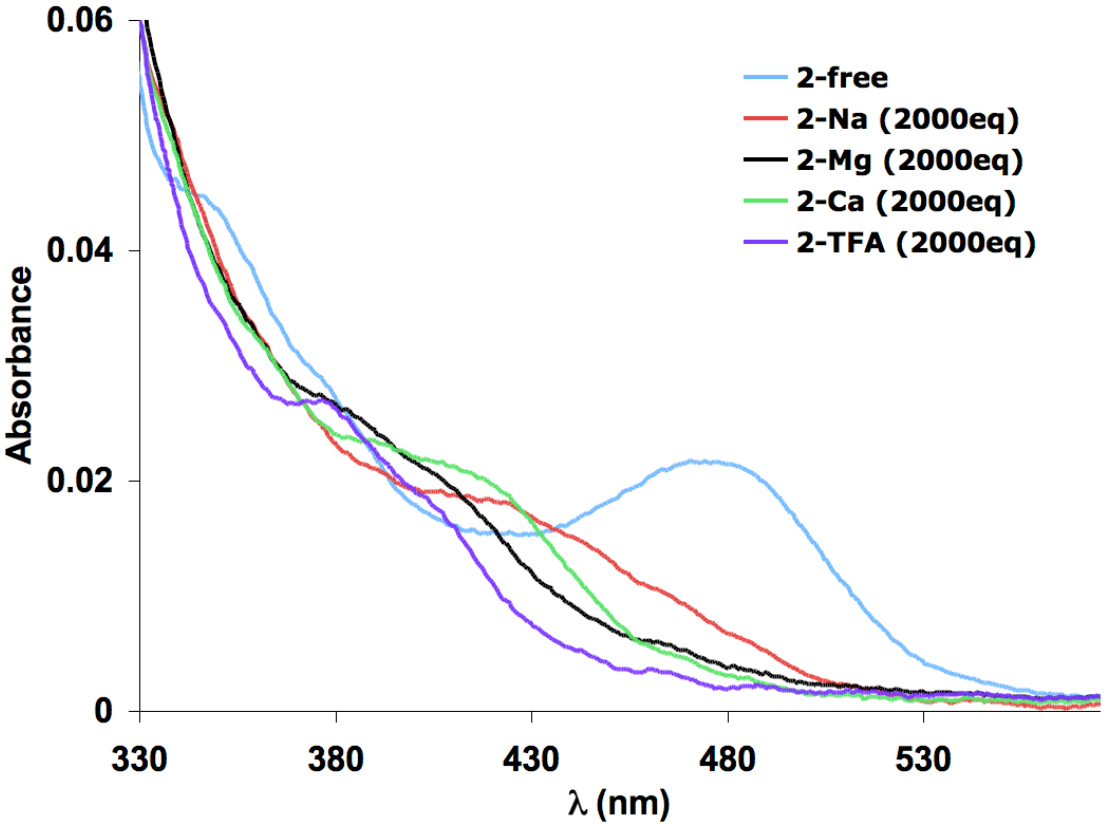

Figure S11. UV-visible spectra of **2** in the presence of excess amounts of metals and TFA. [**2**] = 1.0×10^{-5} M

Quantum yield measurements. The luminescence quantum yields of complexes **1** and **2** and their metal complexes were measured using an absolute method.[iii] Measurements were carried out using a Hamamatsu C9920 system equipped with a xenon lamp, calibrated integrating sphere and model C10027 photonic multichannel analyzer. Dilute solutions (1.0×10^{-5} M) of the compounds in acetonitrile were placed in 1 cm^2 quartz cuvettes, which were fitted with rubber septum and carefully degassed with argon in the dark. The quantum efficiencies were measured using a 380 nm excitation wavelength and the data processed using the U6039-05 software package provided by Hamamatsu. The reproducibility in the quantum efficiency measurements was ± 5%.

Computational methodology. DFT and TD-DFT calculations were performed on model complexes in which the crown ether moiety was replaced by a dimethylamino group for **1** and **2** (**M1**, **M2**) to simplify the calculation without altering the chromophoric part of the receptor. This approach has been adopted successfully in reported semiempirical and TD-DFT calculations.[iv,v] In the same perspective, we used the protonated dimethylamino forms as models for the metallated complexes (**M1-H**, **M2-H**).

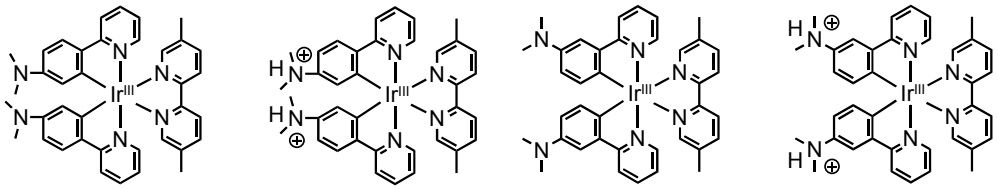

M1 **M1-H** **M2** **M2-H**

Figure S12. Structure of the model complexes

Quantum chemical calculations based on DFT were carried out using the Gaussian03 package.[vi] Ground-state geometry optimizations were performed using the hybrid Hartree Fock/Density functional theory (HF/DFT) method, B3LYP. "Double-ζ" quality basis set consisting of Hay and Wadt's effective core potentials (LANL2DZ) was employed for the iridium(III) atom and 6-31G* basis for H, C, O and N atoms. A relativistic effective core potential (ECP) replaced the inner core electrons of Ir(III), leaving the outer core ($5s^25p^6$) electrons and the $5d^6$ valence electrons. TD-DFT calculations were then carried out on the basis of the optimized ground-state geometry, to calculate the first 20 ground-to-excited state singlet-singlet transition

energies for **M1**, **M1-H**, **M2**, **M2-H** (Figures S13 and S14). The calculated wavelength, oscillator strength and major contributions of the 5 singlet-singlet transitions with highest oscillator strength are given Table S1-S4.

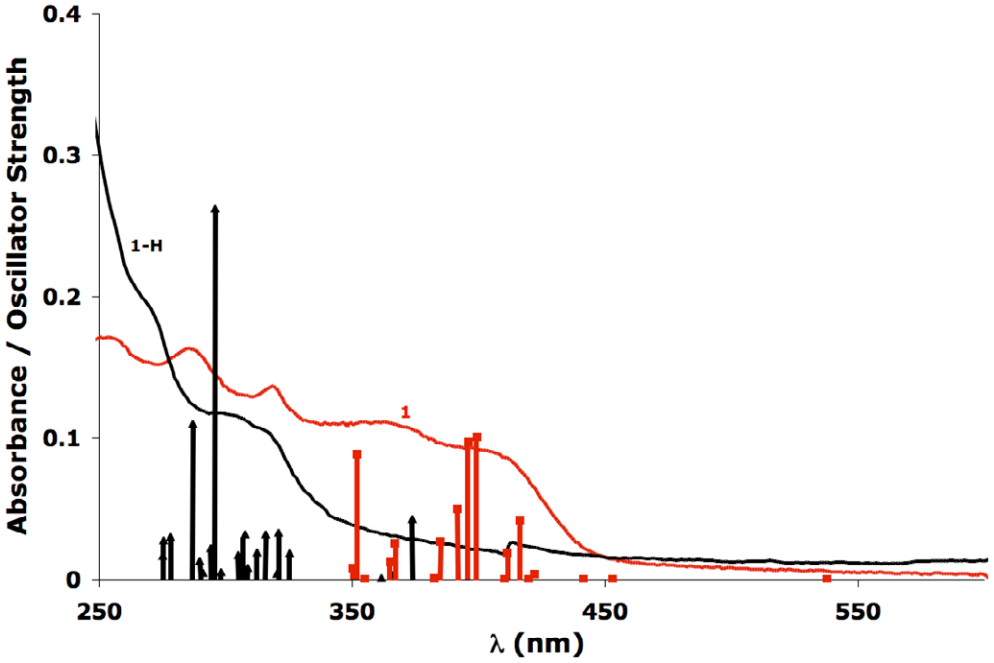

Figure S13. Experimental absorption spectra of **1** (red line) and **1**-H (black line) and TD-DFT-simulated absorption transitions of model complexes **M1** (red sticks) and **M1**-H (black sticks). [**1**] = 1.0×10^{-5} M, CH_3CN.

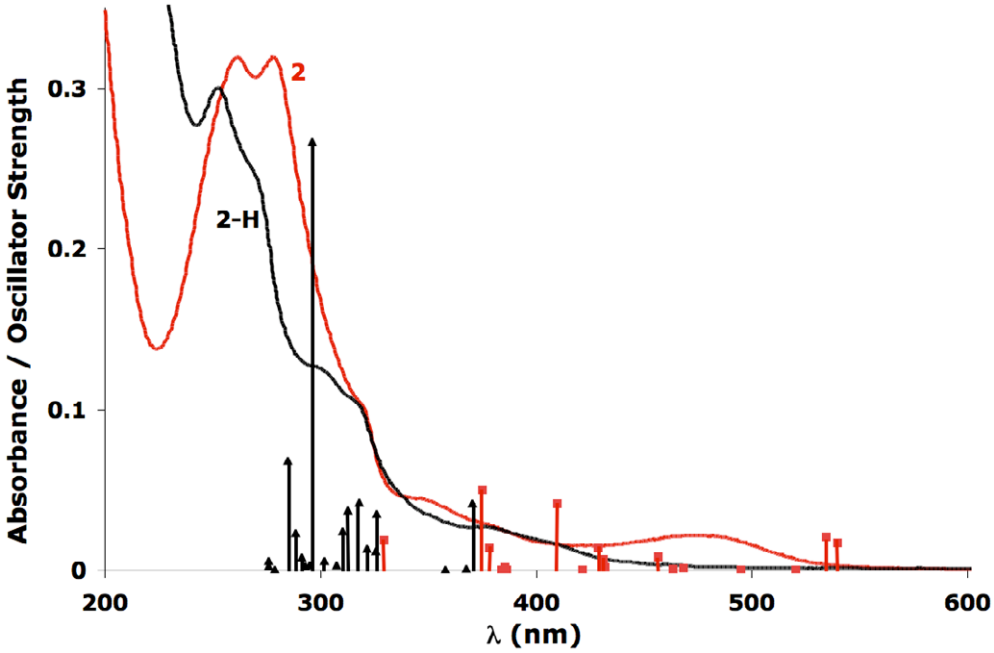

Figure S14. Experimental absorption spectra of **2** (red line) and **2**-H (black line) and TD-DFT-simulated absorption transitions of model complexes **M2** (red sticks) and **M2**-H (black sticks). [**2**] = 1.0×10^{-5} M, CH_3CN.

Table S1. Wavelength, oscillator strength and major contributions of the 5 singlet-singlet transitions (s0-sn) with highest oscillator strength calculated by TD-DFT for **M1**.

No.	Wavelength (nm)	Oscillator Strength	Major contributions
8	416.47	0.0419	HOMO->L+3
11	399.48	0.1004	H-1->L+3
12	396.04	0.0968	H-1->L+4
13	391.62	0.0498	H-5->LUMO
19	352.02	0.0883	HOMO->L+5

Table S2. Wavelength, oscillator strength and major contributions of the 5 singlet-singlet transitions (s0-sn) with highest oscillator strength calculated by TD-DFT for **M1-H**.

No.	Wavelength (nm)	Oscillator Strength	Major contributions
1	373.92	0.043	HOMO->LUMO
5	320.98	0.0334	H-1->L+1
10	307.66	0.0322	H-2->L+1
13	295.75	0.2624	H-3->L+1
17	286.89	0.1105	H-4->L+2

Table S3. Wavelength, oscillator strength and major contributions of the 5 singlet-singlet transitions (s0-sn) with highest oscillator strength calculated by TD-DFT for **M2**.

No.	Wavelength (nm)	Oscillator Strength	Major contributions
3	539.93	0.0169	HOMO->L+1
4	534.62	0.0205	HOMO->L+2
14	409.97	0.0411	H-3->LUMO
19	375.06	0.0501	H-6->LUMO
20	329.52	0.0184	H-2->L+2

Table S4. Wavelength, oscillator strength and major contributions of the 5 singlet-singlet transitions (s0-sn) with highest oscillator strength calculated by TD-DFT for **M2-H**.

No.	Wavelength (nm)	Oscillator Strength	Major contributions
4	326.02	0.0351	H-1->LUMO
7	317.82	0.0424	H-1->L+2
8	312.61	0.0377	H-2->L+2
12	296.02	0.2672	H-3->LUMO
17	284.83	0.0684	H-4->L+2

[i] R. A. Schultz, B. D. White, D. M. Dishong, K. A. Arnold, G. W. Gokel *J. Am. Chem. Soc.*, 1985, **107**, 6659.
[ii] K. Ono, M. Joho, K. Saito, M. Tomura, Y. Matsushita, S. Naka, H. Okada, H. Onnagawa, *Eur. J. Inorg. Chem.*, 2006, 3676.
[iii] Y. Kawamura, H. Sasabe, C. Adachi, *Jpn. J. Appl. Phys., Part 1*, 2004, **43**, 7729.

[iv] M.- L. Ho, Y.- M. Cheng, L.- C. Wu, P.- T. Chou, G.- H. Lee, F.- C. Hsu, H. Chi, *Polyhedron*, 2007, **26**, 4886.
[v] (a) K. Rurack, M. Sczepan, M. Spieles, U. Resch-Genger, W. Rettig, *Chem. Phys. Lett.*, 2000, **320**, 87; (b) L. Antonov, M. Vladimirova, E. Stanoeva, W. M. F. Fabian, L. Ballester, M. Mitewa, *J. Inclusion Phenom. Macrocycl. Chem.*, 2001, **40**, 23.
[vi] M. J. Frisch, G. W. Trucks, H. B. Schlegel, G. E. Scuseria, M. A. Robb, J. R. Cheeseman, J. A. Jr. Montgomery, T. Vreven, K. N. Kudin, J. C. Burant, J. M. Millam, S. S. Iyengar, J. Tomasi, V. Barone, B. Mennucci, M. Cossi, G. Scalmani, N. Rega, G. A. Petersson, H. Nakatsuji, M. Hada, M. Ehara, K. Toyota, R. Fukuda, J. Hasegawa, M. Ishida, T. Nakajima, Y. Honda, O. Kitao, H. Nakai, M. Klene, X. Li, J. E. Knox, H. P. Hratchian, J. B. Cross, V. Bakken, C. Adamo, J. Jaramillo, R. Gomperts, R. E. Stratmann, O. Yazyev, A. J. Austin, R. Cammi, C. Pomelli, J. W. Ochterski, P. Y. Ayala, K. Morokuma, G. A. Voth, P. Salvador, J. J. Dannenberg, V. G. Zakrzewski, S. Dapprich, A. D. Daniels, M. C. Strain, O. Farkas, D. K. Malick, A. D. Rabuck, K. Raghavachari, J. B. Foresman, J. V. Ortiz, Q. Cui, A. G. Baboul, S. Clifford, J. Cioslowski, B. B. Stefanov, G. Liu, A. Liashenko, P. Piskorz, I. Komaromi, R. L. Martin, D. J. Fox, T. Keith, M. A. Al-Laham, C. Y. Peng, A. Nanayakkara, M. Challacombe, P. M. W. Gill, B. Johnson, W. Chen, M. W. Wong, C. Gonzalez, J. A. Pople, *Gaussian 03*, rev C.02; Gaussian, Inc.: Wallingford, CT, 2004.